electronics

MDPI

Article

Wide Voltage Resonant Converter Using a Variable Winding Turns Ratio

Bor-Ren Lin * and Chu-Xian Dai

Department of Electrical Engineering, National Yunlin University of Science and Technology, Yunlin 640, Taiwan; m10812006@yuntech.edu.tw

* Correspondence: linbr@yuntech.edu.tw; Tel.: +886-912312281

Received: 5 February 2020; Accepted: 20 February 2020; Published: 21 February 2020

Abstract: This paper presents a inductor–inductor–capacitor (LLC) resonant converter with variable winding turns to achieve wide voltage operation (100–400 V) and realize soft switching operation over the entire load range. Resonant converters have been developed for consumer power units in computers, power servers, medical equipment, and adaptors due to the advantages of less switching loss and better circuit efficiency. The main disadvantages of the LLC resonant converter are narrow voltage range operation owing to wide switching frequency variation and limited voltage gain. For computer power supplies with hold-up time function, electric vehicle battery chargers, and for power conversion in solar panels, wide input voltage or wide output voltage operation capability is normally demanded for powered electronics. To meet these requirements, the variable winding turns are used in the presented circuit to achieve high- or low-voltage gain when V_{in} is at low- or high-voltage, respectively. Therefore, the wide voltage operation capability can be implemented in the presented resonant circuit. The variable winding turns are controlled by an alternating current (AC) power switch with two back-to-back metal-oxide-semiconductor field-effect transistors (MOSFETs). A 500-W prototype is implemented and test results are presented to confirm the converter performance.

Keywords: pulse frequency control; DC converters; wide voltage operation; zero voltage switching

1. Introduction

Renewable energy systems with electronic power techniques [1–4] have been widely researched to lessen the demands for fossil fuels and reduce the effects of global warming. Form the various renewable energy sources, solar and wind power are more attractive out of the clean energy sources. The main problem with solar and wind power is the non-constant output voltage from wind turbine generators and photovoltaic (PV) solar panels. The output voltage of a wind turbine generator is related to wind speed and the output voltage of a PV solar panel is related to solar intensity. High-efficiency direct current (DC) power converters [5–8] have been proposed for power units for computers, battery dischargers and chargers, telecommunication systems, and server systems. Out of the various soft switching techniques, the active clamp technique [9,10], asymmetric pulse width modulation (PWM) [11,12], and phase-shift PWM converters [13,14] are the most attractive circuit topologies with the lowest switching losses. The PWM scheme is widely used to control these circuit topologies with constant output voltage. However, the turn-on time of the PWM scheme is dependent on the input voltage. PWM converters have a low (high) duty cycle at high (low) voltage input. However, the low duty cycle results in a high root mean square current and high conduction loss. Thus, the PWM converters have low (high) circuit efficiency at high (low) input voltage conditions. This drawback limits PWM converters in terms of wide voltage operation. Pulse frequency modulation (PFM), or variable frequency control, has been adopted in resonant converters [15]. In many resonant circuit topologies, the inductor–inductor–capacitor (LLC) resonant converter is a more attractive circuit

topology for use in high-input voltage inputs. The main advantages of LLC resonant converters [16–18] are low switching loss in power devices, high efficiency, and low electromagnetic interference (EMI). The main drawback of LLC resonant converters is the limited voltage gain. This means it is difficult to operate the resonant converter in wide voltage operation. To realize wide voltage operation, two-stage converters and series–parallel connection for full-bridge or half-bridge converters [19–22] have been proposed for battery charger, solar power, and wind power applications. The two-stage converters have the drawback of low efficiency, while the series- or parallel-connected converters have more circuit components, which increase the conduction loss and reduce the converter reliability. In [23,24], two full-bridge LLC converters with primary-parallel–secondary-series connection were proposed to achieve wide input or output voltage operation. However, eight power switches and eight diodes are used in this circuit topology. The conduction losses in power semiconductors and the cost are increased. An interleaved LLC resonant converter has been studied and implemented in [25] to realize wide input voltage operation and ripple-free input current. However, this circuit topology is a two-stage circuit structure, meaning that the circuit efficiency is low in full load conditions, when both the boost converter and LLC converter are operated. In [26], a half-bridge LLC resonant converter with two sets of center-tapped rectifiers was proposed to extend the hold-up time problem for personal computers. However, four winding turns are used on the secondary side in this circuit topology, and the copper losses on magnetic windings are increased.

An LLC resonant converter with variable winding turns is proposed and investigated to achieve soft switching operation on active switches over the entire load range and for wide voltage range operation (V_{in} = 100–400 V). The variable winding turns controlled by an alternating current (AC) switch are adopted to achieve different voltage gains based on low- or high-input voltage ranges. During the low-input voltage range (from V_{in} = 100 V to 200 V), the converter with more secondary turns is selected to achieve high-voltage gain for the LLC converter. During the input voltage range (V_{in} = 200–400 V), the converter with fewer secondary turns is operated to achieve low-voltage gain for the LLC converter. Therefore, the proposed converter can be operated under wide input voltage variation, such as for solar power or switching mode power supplies without power factor correction, under the universal AC input voltage. The LLC resonant circuit with pulse-frequency modulation is used to control active devices. Due to the inductive impedance load of the LLC resonant tank, the converter can realize soft switching operation for both active switches and rectifier diodes. The voltage double rectifier topology is adopted on the output side to limit the voltage rating of the secondary diodes at V_o instead of $2V_o$ in center-tapped rectifiers. The rectifier diodes with a low-voltage rating have low-voltage drop. Comparing the center-tapped rectifier structure, the voltage double rectifier structure has less conduction losses for rectifier diodes and secondary windings. Comparing the conventional two-stage power converters, parallel-series connected converters, and the other resonant converters in [19–26], the presented LLC resonant converter has a simple circuit structure, a simple control algorithm, and requires fewer power components to achieve wide voltage operation. The description of the presented circuit schematic and operation principle is presented in Section 2. The circuit analysis and design procedures of the presented resonant converter are provided in Section 3. Experiments are demonstrated and discussed to confirm the effectiveness of the presented converter in Section 4. Finally, the conclusions are discussed in Section 5.

2. Proposed Converter and Operation Principle

Figure 1a shows the conventional LLC converter. The half-bridge leg and center-tapped rectifier are used on the primary and secondary sides, respectively, for high-voltage input and low-voltage output applications. According to the center-tapped rectifier topology, the secondary diodes have $2V_o$ voltage stress. Figure 1b shows the circuit topology with the voltage double rectifier for medium- or high-voltage output applications. The advantages of this circuit topology are the low-voltage rating of the rectifier diodes ($V_{D1,\text{rating}} = V_{D1,\text{rating}} = V_o$) and fewer secondary winding turns (n_s instead of $2n_s$)

in the center-tapped rectifier structure. Therefore, the voltage double rectifier structure has less copper loss on the secondary windings.

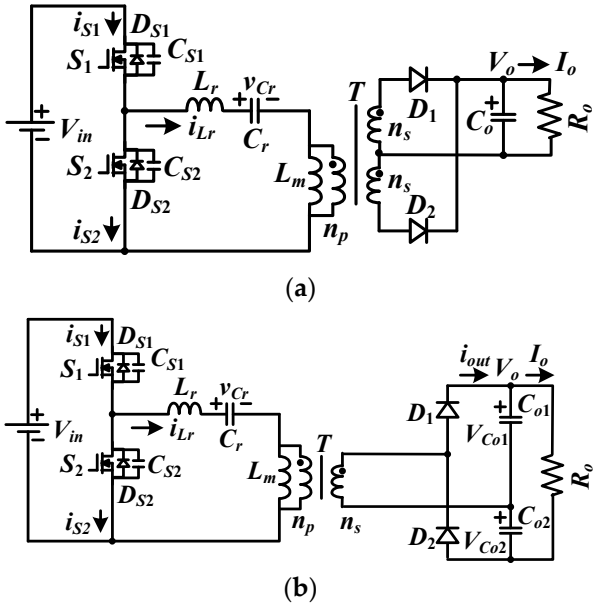

Figure 1. Conventional inductor–inductor–capacitor (LLC) converter based on (**a**) a center-tapped rectifier structure and (**b**) a voltage double rectifier structure.

In order to improve the drawback of the limit voltage range in conventional LLC converters, Figure 2a shows the circuit configuration of the presented LLC converter with variable winding turns to achieve wide input voltage operation (100–400 V). The input voltage of the proposed LLC converter can be from the output of the solar panels, wind turbine DC generators, or battery banks. The output voltages of battery banks and large solar panels vary widely. A half-bridge LLC resonant tank is used on the primary side for soft switching operation in active devices S_1 and S_2 over the entire load range. The voltage rating of the active devices equals the maximum input voltage. Two sets of voltage double rectifiers and one AC switch S_{ac} implemented with two metal-oxide-semiconductor field-effect transistors (MOSFETs) back-to-back connection are used on the output-side. If the proposed converter is operated under low-voltage input $V_{in,L}$ (100–200 V), then S_{ac} is turned on (Figure 2b). Due to S_{ac} is conducting, the $2n_s$ secondary winding turns are connected to load voltage. One observes that D_3 and D_4 are off. The transformer turns-ratio under low-input voltage operation is $n_p/(2n_s)$. The proposed converter has DC voltage gain $V_o/V_{in,L} = G(f)(2n_s)/n_p$, where $V_{in,L}$ and G (f) are low-input voltage range and the voltage transfer function of LLC converter. When the circuit is worked under high-voltage range $V_{in,H}$ (200–400 V), S_{ac} is controlled at off state (Figure 2c). The n_s winding turns are connected to load voltage and the diodes D_1 and D_2 are off. Therefore, the transformer turns-ratio for high-voltage operation is equal to n_p/n_s. The direct current voltage gain $V_o/V_{in,H}$ of the LLC converter is $G(f)n_s/n_p$, where $V_{in,H}$ is high-input voltage range. From the previous discussion, one can observe that $V_o/V_{in,L} = G(f)(2n_s)/n_p = 2V_o/V_{in,H}$. It is concluded that $V_{in,H} = 2V_{in,L}$, such as $V_{in,H}$ = 200–400 V and $V_{in,L}$ = 100–200 V. Therefore, the presented resonant converter has high (low) DC voltage gain operated at low (high) input voltage range with low (high) transformer turns-ratio. The PWM signals of S_1 and S_2 are controlled with pulse-frequency modulation scheme shown in Figures 3a and 4a and the AC switch S_{ac} is controlled by the Schmitt voltage comparator. The reference voltage of the Schmitt voltage comparator is 200 V and the hysteresis voltage band is 10 V.

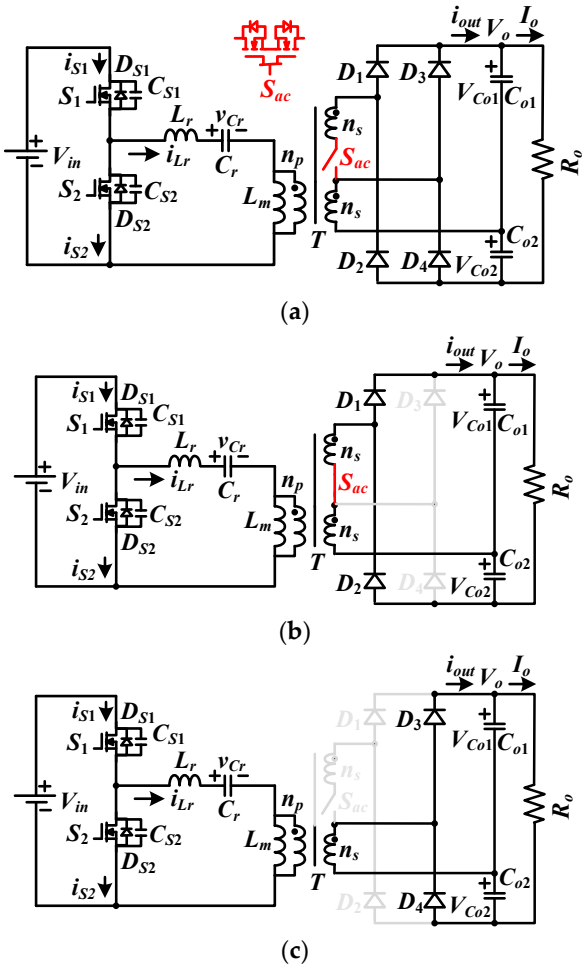

Figure 2. Circuit structure of (**a**) the presented converter (**b**) under low-voltage operation (S_{ac} on) and (**c**) under high-voltage operation (S_{ac} off).

2.1. Low-Voltage Operation $V_{in,L} = V_{in,min}$–$2V_{in,min}$ (S_{ac}: on, D_3, D_4: off)

If the converter is operated at the low-voltage input from $V_{in,min}$ to $2V_{in,min}$, then S_{ac} is turned on and D_3 and D_4 are turned off. The proposed converter has a DC voltage gain of $V_o/V_{in,L} = G(f)(2n_s)/n_p$. According to the switching states of S_1, S_2, D_1, and D_2, the converter has six operating modes for each switching cycle. The PWM waveforms are demonstrated in Figure 3a. Figure 3b–g gives the equivalent circuits of six operating modes under f_{r1} (series resonant frequency) > f_{sw} (switching frequency).

Mode 1 [$t_0 \sim t_1$]: This mode begins at t_0 if $v_{CS1} = 0$ V and $v_{CS2} = V_{in}$. Owing to $i_{Lr}(t_0) < 0$ and $i_{Lr} > i_{Lm}$, the body diode D_{S1} conducts and D_1 is forward-biased. Switch S_1 turns on after t_0 to achieve zero voltage switching. The magnetizing voltage $v_{Lm} = n_p V_{Co1}/(2n_s) = n_p V_o/(4n_s)$ and the magnetizing current i_{Lm} increase in this mode. In mode 1, the series resonant frequency is $f_{r1} = 1/2\pi\sqrt{L_r C_r}$. If f_{r1} (series resonant frequency) < f_{sw} (switching frequency), then the circuit goes to mode 3. Otherwise, the circuit goes to mode 2 at time t_1.

Mode 2 [$t_1 \sim t_2$]: At t_1, $i_{D1} = 0$ and D_1 turns off without the reverse recovery current. In mode 2, the resonant frequency is $f_{r2} = 1/2\pi\sqrt{(L_r + L_m)C_r}$. It is clear that the resonant frequency f_{r2} in mode 2 is less than the frequency f_{r1} in mode 1. The peak-to-peak current of L_m is approximately obtained as

$$\Delta i_{Lm} \approx \frac{n_p V_o}{8 n_s L_m f_{sw}} \tag{1}$$

Thus, the magnetizing current at time t_2 is given as

$$i_{Lm}(t_2) = \frac{\Delta i_{Lm}}{2} \approx \frac{n_p V_o}{16 n_s L_m f_{sw}} \tag{2}$$

Mode 3 [$t_2 \sim t_3$]: This mode starts at t_2 when switch S_1 is turned off. Owing to $i_{Lr}(t_2) > 0$ and $i_{Lr} < i_{Lm}$, C_{S2} (C_{S1}) is discharged (charged) from V_{in} (0 V) and D_2 is forward-biased. If the inductor energy E_{Lr+Lm} at time t_2 is larger than the capacitor energy $E_{CS1+CS2}$, then v_{Cs2} will be decreased to zero voltage at time t_3. The zero voltage switching condition of S_2 is expressed as

$$i_{Lm}(t_2) \geq V_{in} \sqrt{2C_{oss}/(L_m + L_r)} \tag{3}$$

where $C_{oss} = C_{S1} = C_{S2}$. The dead time ($t_d$) between S_1 and S_2 must be greater than the discharge time of C_{S2} to ensure the zero voltage turn-on of S_2. Thus, the maximum value of L_m can be calculated as

$$L_m \leq \frac{n_p V_o t_d}{32 V_{in} f_s n_s C_{oss}} \tag{4}$$

Mode 4 [$t_3 \sim t_4$]: At time t_3, $v_{CS2} = 0$ V and $v_{CS1} = V_{in}$. Owing to $i_{Lr}(t_3) > 0$ and $i_{Lr} < i_{Lm}$, the body diode D_{S2} conducts and D_2 is forward-biased. S_2 can turn on after t_3 with soft switching operation. In mode 4, $v_{Lm} = -n_p V_{Co2}/(2n_s) = -n_p V_o/(4n_s)$ and i_{Lm} decreases. The resonant frequency in mode 4 is f_{r1}. If $f_{sw} < f_{r1}$, then $i_{D2} = 0$ at time t_4.

Mode 5 [$t_4 \sim t_5$]: At t_4, $i_{D2} = 0$ and D_2 turns off without the reverse recovery current. L_r, L_m, and C_r are naturally resonant with the frequency f_{r2}.

Mode 6 [$t_5 \sim T_{sw}+t_0$]: At t_5, S_2 is turned off. Owing to $i_{Lr}(t_5) < 0$ and $i_{Lr} > i_{Lm}$, C_{S1} is discharged and D_1 is forward-biased. The soft switching turn-on condition of S_1 is expressed as

$$|i_{Lm}(t_5)| = i_{Lm}(t_2) \geq V_{in} \sqrt{2C_{oss}/(L_m + L_r)} \tag{5}$$

At time $t_0 + T_{sw}$, $v_{CS1} = 0$ V.

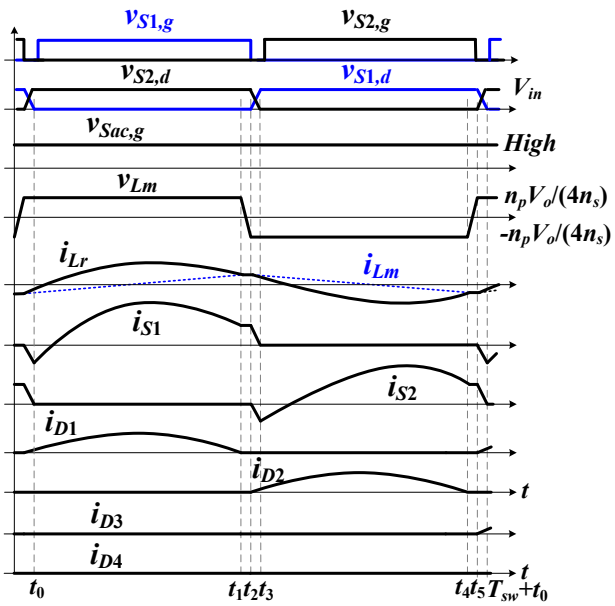

(**a**)

Figure 3. *Cont.*

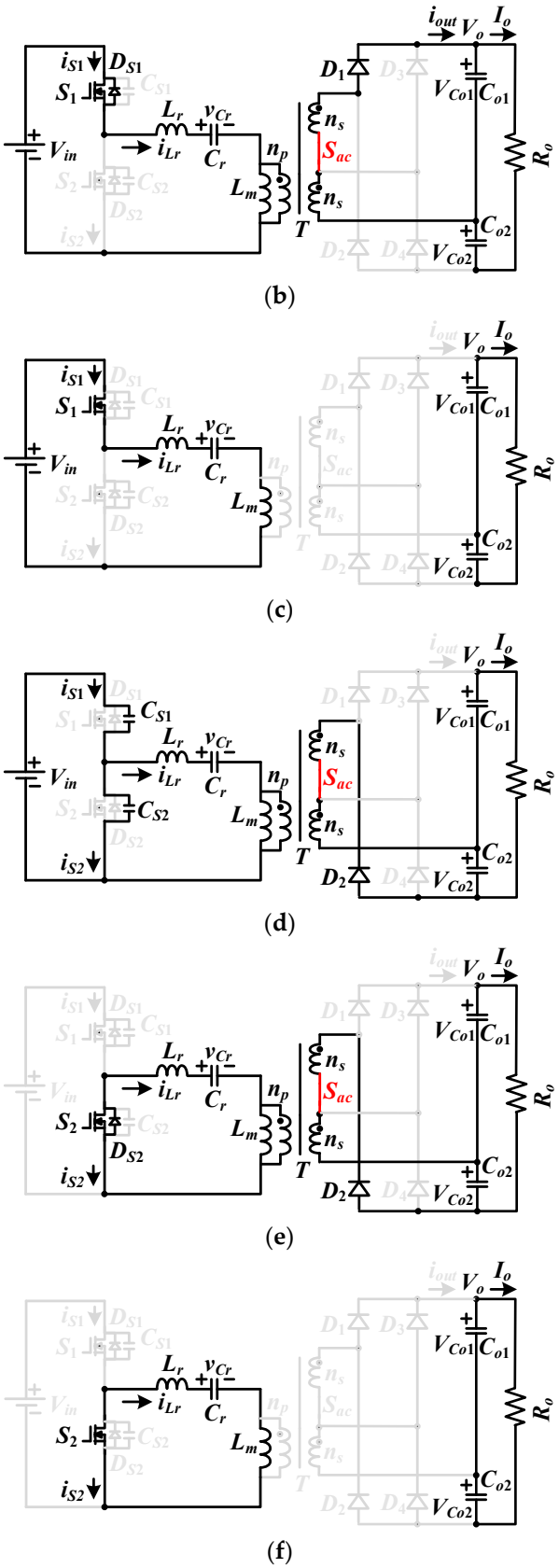

Figure 3. *Cont.*

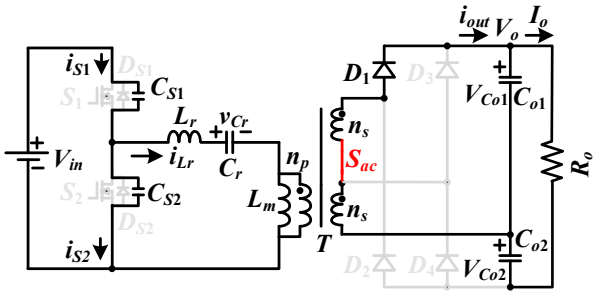

Figure 3. LLC circuits operated at low-input voltage ranges: (**a**) pulse width modulation PWM waveforms; (**b**) mode 1; (**c**) mode 2; (**d**) mode 3; (**e**) mode 4; (**f**) mode 5; (**g**) mode 6.

2.2. High-Voltage Operation $V_{in,H} = 2V_{in,min}$–$4V_{in,min}$ (S_{ac}: off, D_1, D_2: off)

If the converter is worked at the high-voltage input from $2V_{in,min}$ to $4V_{in,min}$, then S_{ac} turns off, and D_1 and D_2 are also off. The DC voltage gain becomes $V_o/V_{in,H} = G(f)n_s/n_p$. According to the on–off states of S_1, S_2, D_3, and D_4, the LLC converter has six operating modes for each switching period. Figure 4 gives the PWM waveforms and equivalent circuits under high-input voltage operation.

Mode 1 [$t_0 \sim t_1$]: At time t_0, $v_{CS1} = 0$ V. Since $i_{Lr} > i_{Lm}$ and $i_{Lr}(t_0) < 0$, D_{S1} is forward-biased and D_3 conducts. Thus, the zero voltage turn-on of S_1 can be realized after t_0. Due to D_3 being forward-biased, one can obtain $v_{Lm} = n_p V_{Co1}/n_s = n_p V_o/(2n_s)$ and i_{Lm} increases. The resonant frequency in mode 1 is $f_{r1} = 1/2\pi\sqrt{L_r C_r}$.

Mode 2 [$t_1 \sim t_2$]: At time t_1, $i_{D3} = 0$ and D_3 turns off at t_1 without the reverse recovery current. The resonant frequency in mode 2 is $f_{r2} = 1/2\pi\sqrt{(L_r + L_m)C_r}$. The peak-to-peak ripple current ΔL_m and the magnetizing current at time t_2 are approximately calculated as

$$\Delta i_{Lm} \approx \frac{n_p V_o}{4 n_s L_m f_{sw}} \tag{6}$$

$$i_{Lm}(t_2) = \frac{\Delta i_{Lm}}{2} \approx \frac{n_p V_o}{8 n_s L_m f_{sw}} \tag{7}$$

Mode 3 [$t_2 \sim t_3$]: At t_2, S_1 turns off. Due to $i_{Lr} < i_{Lm}$ and $i_{Lr}(t_2) > 0$, D_4 conducts and C_{S2} is discharged from V_{in}. If the inductor energy on L_r and L_m is larger than the capacitor energy on C_{S1} and C_{S2}, then v_{CS2} is decreased to zero voltage at t_3. The zero voltage turn-on condition of S_2 is expressed as

$$i_{Lm}(t_2) = \frac{n_p V_o}{8 n_s L_m f_{sw}} \geq V_{in}\sqrt{2C_{oss}/(L_m + L_r)} \tag{8}$$

If the dead time (t_d) between S_1 and S_2 is given, the maximum value of L_m under the high-input voltage range is obtained as

$$L_m \leq \frac{n_p V_o t_d}{16 V_{in} f_s n_s C_{oss}} \tag{9}$$

Mode 4 [$t_3 \sim t_4$]: At t_3, $v_{CS2} = 0$. Owing to $i_{Lm} > i_{Lr}$ and $i_{Lr}(t_3) > 0$, D_4 conducts and D_{S2} is forward-biased. Therefore, the zero voltage turn-on of S_2 can be achieved. Due to D_4 conducting, one can obtain $v_{Lm} = -n_p V_{Co2}/n_s = -n_p V_o/(2n_s)$ and i_{Lm} decreases in this mode. The resonant frequency in this mode is f_{r1}.

Mode 5 [$t_4 \sim t_5$]: At time t_4, $i_{D4} = 0$ and D_4 turns off without the reverse recovery current. The resonant frequency in mode 5 equals f_{r2}.

Mode 6 [$t_5 \sim T_{sw}+t_0$]: At time t_5, S_2 turns off. Since $i_{Lm} < i_{Lr}$ and $i_{Lr}(t_5) < 0$, D_3 is forward-biased and C_{S1} is discharged. The zero voltage turn-on condition of S_1 is expressed as

$$|i_{Lm}(t_5)| = i_{Lm}(t_2) = \frac{n_p V_o}{8 n_s L_m f_{sw}} \geq V_{in}\sqrt{2C_{oss}/(L_m + L_r)} \tag{10}$$

At $t_0 + T_{sw}$, $v_{CS1} = 0$.

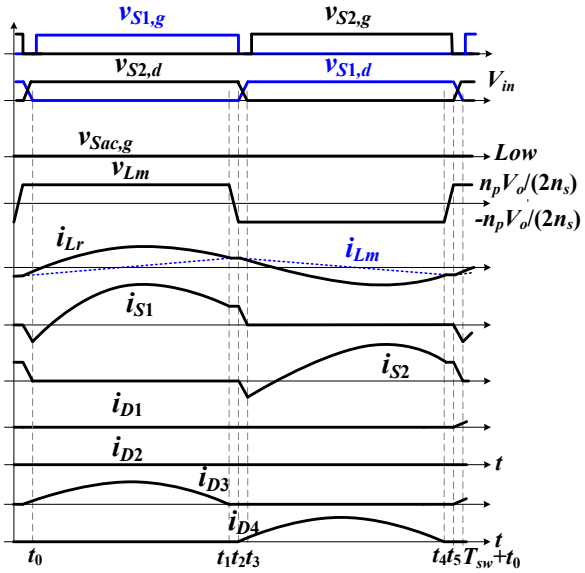

(**a**)

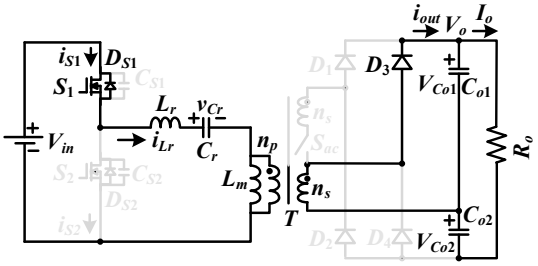

(**b**)

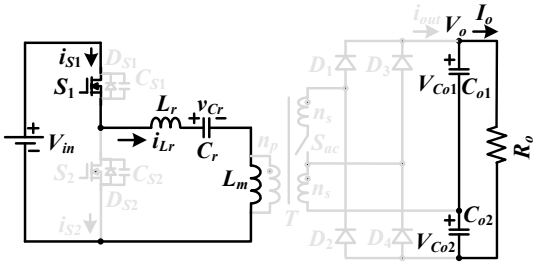

(**c**)

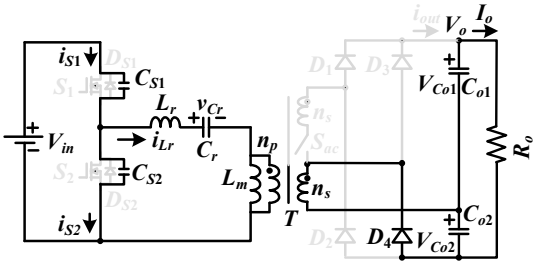

(**d**)

Figure 4. *Cont.*

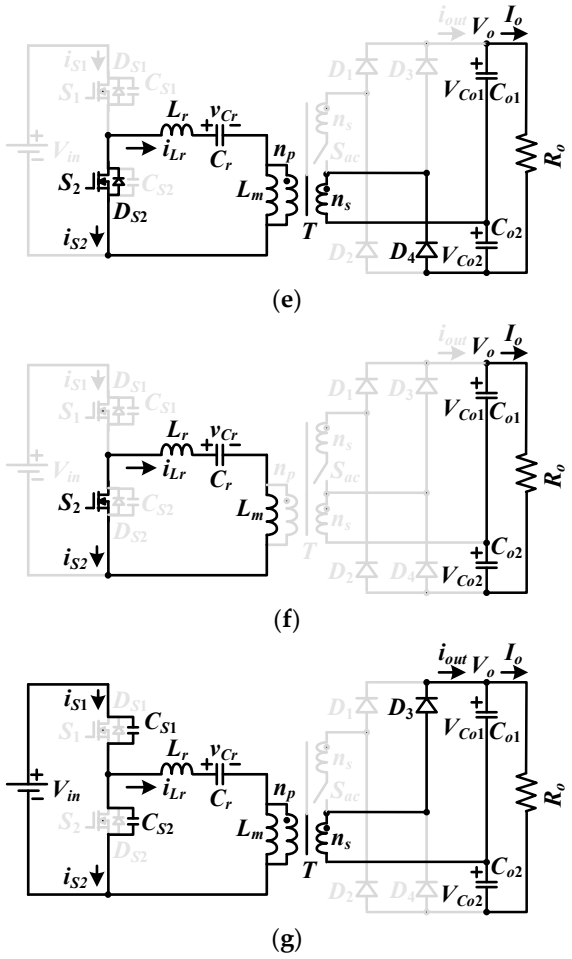

Figure 4. LLC circuits operated at high-input voltage ranges: (**a**) PWM waveforms; (**b**) mode 1; (**c**) mode 2; (**d**) mode 3; (**e**) mode 4; (**f**) mode 5; (**g**) mode 6.

3. Circuit Analysis and Design Procedure

The presented LLC converter is operated with pulse frequency modulation (PFM). Power switches have a constant duty cycle ($d = 0.5$) with variable frequency. The switching frequency is dependent on V_{in} and P_o. The fundamental harmonic frequency approach is used to analyze the circuit characteristics. The variable winding turns controlled by the AC switch S_{ac} are used on the secondary side to adjust the voltage gain under low- or high-voltage input. Based on the fundamental harmonic frequency analysis, the AC equivalent circuit of the resonant tank is given in Figure 5. R_e is the equivalent primary side resistor of transformer. Since the PWM signals of S_1 and S_2 are square waves with duty cycle $d = 0.5$, the input voltage of the LLC circuit becomes a square voltage wave measuring 0 V (if S_2 is on) or V_{in} (if S_1 is on). The fundamental root mean square (*rms*) input voltage is calculated as $\sqrt{2}V_{in}/\pi$. Since S_{ac} is turned on at low-voltage inputs and off at high-voltage inputs, the secondary winding turns $2n_s$ (n_s) are connected to the output load under low (high) input voltage ranges. The primary side magnetizing voltage is a square wave with a voltage value of $v_{Lm} = \pm n_p V_o/(4n_s)$ if S_{ac} is conducting or $v_{Lm} = \pm n_p V_o/(2n_s)$ if S_{ac} is off. The fundamental *rms* voltage $V_{Lm,rms}$ is calculated as $n_p V_o/(\sqrt{2}\pi n_s)$ for low-input voltage ranges or $\sqrt{2}n_p V_o/(\pi n_s)$ for high-input voltage operation. The DC load resistor R_o is reflected to the primary side of the transformer and the AC equivalent resistor R_e can be obtained

as $R_e = \left(n_p/n_s\right)^2 R_o/(2\pi^2)$ for low-voltage ranges or $R_e = 2\left(n_p/n_s\right)^2 R_o/\pi^2$ for high-voltage ranges. The voltage transfer function in Figure 5 is calculated as

$$|G| = 1/\sqrt{X^2\left(\frac{F_n^2-1}{F_n}\right)^2 + \left[1+\frac{1}{L_n}\frac{F_n^2-1}{F_n^2}\right]^2} = \begin{cases} \frac{n_p V_o}{2n_s V_{in}}, & \text{if } S_{ac} \text{is on} \\ \frac{n_p V_o}{n_s V_{in}}, & \text{if } S_{ac} \text{is off} \end{cases} \quad (11)$$

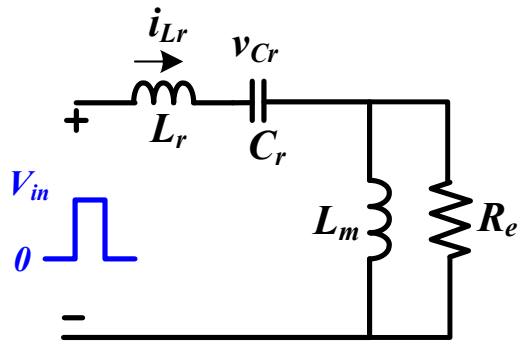

Figure 5. Alternating current (AC) equivalent circuit of the resonant tank.

Here, $X = \sqrt{L_r/C_r}/R_e$, $F_n = f_{sw}/f_r$ and $L_n = L_m/L_r$. From Equation (11), the output voltage is obtained as

$$V_o == \begin{cases} \frac{2n_s V_{in}}{n_p\sqrt{X^2\left(\frac{F_n^2-1}{F_n}\right)^2+\left[1+\frac{1}{L_n}\frac{F_n^2-1}{F_n^2}\right]^2}}, & \text{if } S_{ac} \text{ is on} \\ \frac{n_s V_{in}}{n_p\sqrt{X^2\left(\frac{F_n^2-1}{F_n}\right)^2+\left[1+\frac{1}{L_n}\frac{F_n^2-1}{F_n^2}\right]^2}}, & \text{if } S_{ac} \text{ is off} \end{cases} \quad (12)$$

Power switches S_1 and S_2 are controlled with pulse frequency modulation and the LLC converter is operated over wide voltage ranges.

The design procedures of prototypes are provided to confirm the feasibility of the presented LLC converter. The input voltage range V_{in} is from 100 to 400 V, the output voltage V_o is 48 V, the full power $P_{o,rated}$ is 500 W, and the series resonant frequency f_{r1} is 100 kHz. The inductance ratio L_n is assumed as 7. When V_{in} = 100–200 V, the proposed converter is operated at low-voltage ranges. If V_{in} = 200–400 V, then the proposed LLC converter is worked under high-voltage ranges. Since the proposed converter has the same resonant tank under high and low-voltage ranges, the prototype circuit can be designed for either high- or low-input voltage ranges. For high-voltage range operation, the minimum voltage gain of the presented LLC converter under $V_{in,max}$ = 400 V is assumed at unity. Then, the turns ratio n_p/n_s is expressed in Equation (13) as

$$\frac{n_p}{n_s} = \frac{GV_{in,\max}}{V_o} = \frac{1\times 400}{48} \approx 8.33 \quad (13)$$

The magnetic core TDK EE-55 with ΔB = 0.4 T and A_e = 354 mm^2 is adopted to implement transformer T. It is assumed that the minimum switching frequency is 50 kHz under V_{in} = 200 V conditions. Therefore, the minimum primary winding turns are calculated as

$$n_{p,\min} \geq \frac{(n_p/n_s)V_o}{4f_{s,\min}\Delta B A_e} = \frac{(8.333)\times 48}{4\times 50000\times 0.4\times 354\times 10^{-6}} \approx 14.123 \quad (14)$$

In the laboratory prototype, we selected n_p = 16 and n_s = 2. Thus, the actual DC gains are obtained in Equations (15) and (16) as

$$G_{\max,H} = \frac{V_o n_p}{V_{in,\min} n_s} = \frac{48\times 16}{200\times 2} \approx 1.92 \quad (15)$$

$$G_{\min,H} = \frac{V_o n_p}{V_{in,\max} n_s} = \frac{48 \times 16}{400 \times 2} \approx 0.96 \tag{16}$$

Similarly, the DC voltage gains of the presented resonant converter for low-voltage ranges are obtained as

$$G_{\max,L} = \frac{V_o n_p}{2V_{in,\min} n_s} = \frac{48 \times 16}{2 \times 100 \times 2} \approx 1.92 \tag{17}$$

$$G_{\min,L} = \frac{V_o n_p}{2V_{in,\max} n_s} = \frac{48 \times 16}{2 \times 200 \times 2} \approx 0.96 \tag{18}$$

From the calculated winding turns n_p and n_s, the equivalent resistance R_e at high-voltage ranges and the rated power are calculated as

$$R_e = \frac{2(n_p/n_s)^2 R_o}{\pi^2} = \frac{2 \times (16/2)^2 \times (48^2/500)}{3.14159^2} \approx 60\ \Omega \tag{19}$$

The quality factor X is selected as 0.2. The resonant inductor L_r is calculated as

$$L_r = \frac{xR_e}{2\pi f_{r1}} = \frac{0.2 \times 60}{2\pi \times 100000} \approx 19\ \mu\text{H} \tag{20}$$

In the proposed converter, the actual resonant inductance L_r is 20 µH. Then, the resonant capacitor is calculated as

$$C_r = \frac{1}{4\pi^2 L_r f_{r1}^2} = \frac{1}{4\pi^2 \times 20 \times 10^{-6} \times (100000)^2} \approx 127\ \text{nF} \tag{21}$$

Since the selected $L_n = L_m/L_r = 7$, the magnetizing inductance L_m is obtained as

$$L_m = L_n L_r = 7 \times 20 = 140\ \mu\text{H} \tag{22}$$

MBR40100PT diodes with a 100 V/40 A rating are used for D_1–D_4. The selected output capacitance $C_{o1} = C_{o2} = 540$ µF/100 V. The Schmitt voltage comparator with a reference voltage of 200 V is used to control switch S_{ac}. Switch S_{ac} is implemented by two IRF1405ZPBF metal-oxide-semiconductor field-effect transistors (MOSFETs) with a 55 V/118 A rating. The voltage stress of S_1 and S_2 is $V_{in,max} = 400$ V. In the prototype, STW48N60M2 MOSFETs with a 600 V/26 A rating are used for S_1 and S_2. The UCC25600 PWM integrated circuit is adopted to realize pulse frequency modulation. The voltage TL431 regulator and the PC 817 optocoupler are adopted on the low-voltage side to achieve load voltage regulation and signal isolation, respectively. Figure 6 provides the circuit diagram of the prototype with the adopted control scheme.

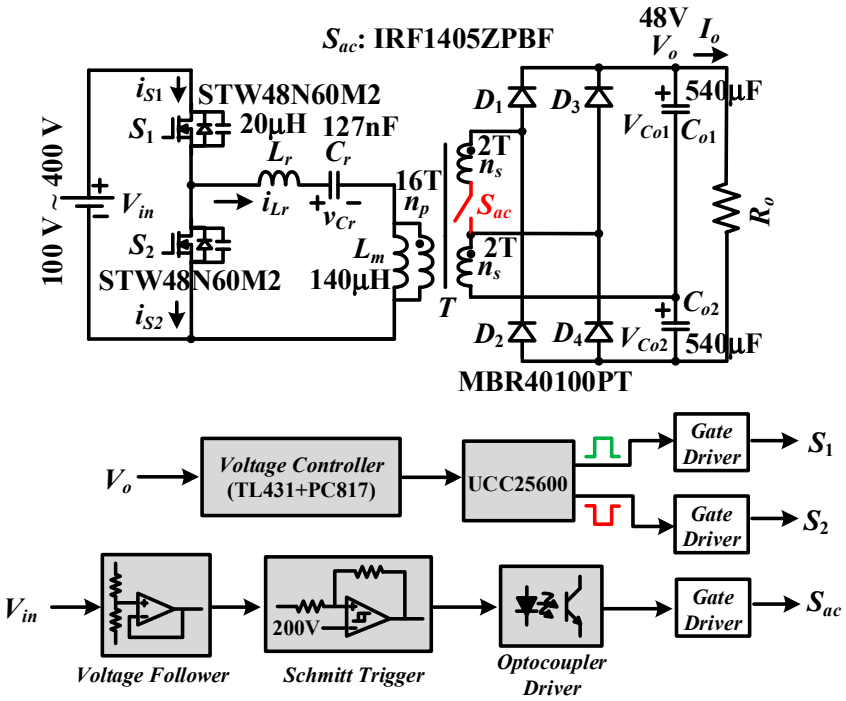

Figure 6. Circuit diagram of the laboratory prototype.

4. Experimental Results

The measured waveforms of the prototype circuit are given to confirm the effectiveness of the presented LLC resonant converter with wide voltage operation. The experimental waveforms of $v_{S1,g}$, $v_{S2,g}$, v_{Cr}, and i_{Lr} for different input voltages 100 V, 190 V, 210 V, and 400 V are given in Figure 7. For V_{in} = 100 V and 190 V, the presented converter is operated at low-voltage ranges. The S_{ac} conducts and $2n_s$ winding turns are connected to the output load. The converter operated at V_{in} = 100 V has high-voltage gain compared to the converter operated at V_{in} = 190 V. One can observe that the switching frequency of the converter at V_{in} = 190 V is greater than the switching frequency at V_{in} = 100 V. For V_{in} = 210 V and 400 V conditions, the presented LLC converter is operated at high-voltage ranges. The S_{ac} is turned off and n_s instead of $2n_s$ winding turns are connected to the output load. Similarly, the proposed converter operated at V_{in} = 210 V has a lower switching frequency compared to the converter operated at V_{in} = 400 V. The experimental waveforms of i_{D1}–i_{D4} for different input voltage conditions and the full power are given in Figure 8. For V_{in} = 100 V and 190 V conditions, the switch S_{ac} is turned on and D_3 and D_4 are reverse-biased. Therefore, $i_{D3} = i_{D4} = 0$, as shown in Figure 8a,b. On the other hand, S_{ac} is turned off, while D_1 and D_2 are also off for V_{in} = 210 V and 400 V conditions. Therefore, $i_{D1} = i_{D2} = 0$, as shown in Figure 8c,d. Diodes D_1 and D_2 turn off without the reverse recovery current at V_{in} = 100 V (Figure 8a) because f_{sw} at V_{in} = 100 V is about 45 kHz < f_{r1} = 100 kHz. Similarly, D_3 and D_4 also turn off without the reverse recovery current at V_{in} = 210 V (Figure 8c) because f_{sw} is about 50 kHz < f_{r1} = 100 kHz. The experimental waveforms of switch S_1 at 20% power and different input voltage conditions are given in Figure 9. The experimental waveforms of S_1 at 100% power and different input voltage conditions are illustrated in Figure 10. From the experimental waveforms in Figure 9; Figure 10, it is clear that S_1 is turned when zero voltage switches from 20% power to 100% power and over the entire voltage range.

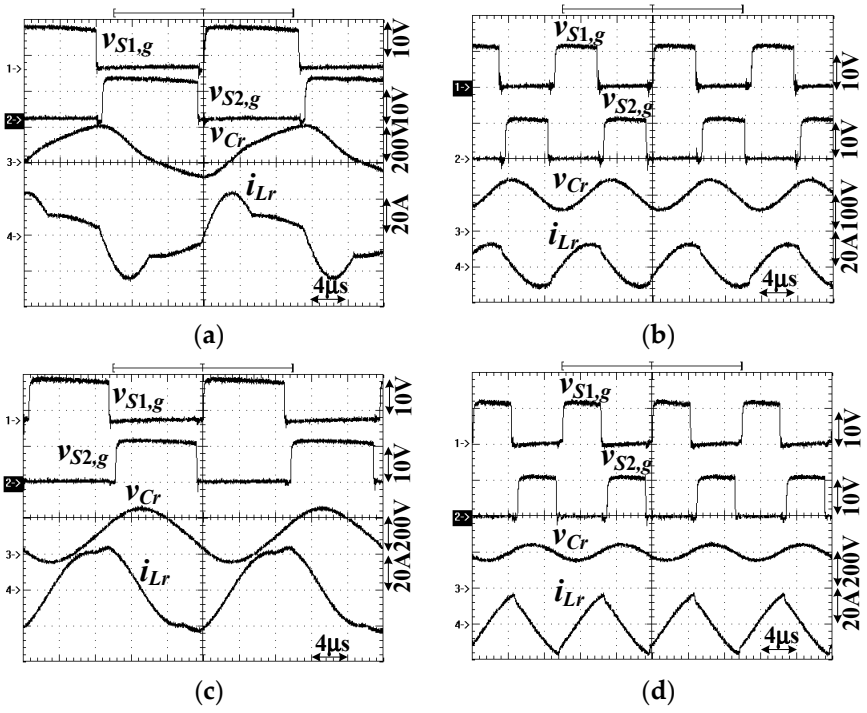

Figure 7. Measured results of $v_{S1,g}$, $v_{S2,g}$, v_{Cr}, and i_{Lr} at rated power values of:(**a**) V_{in} = 100 V; (**b**) V_{in} = 190 V; (**c**) V_{in} = 210 V; (**d**) V_{in} = 400 V.

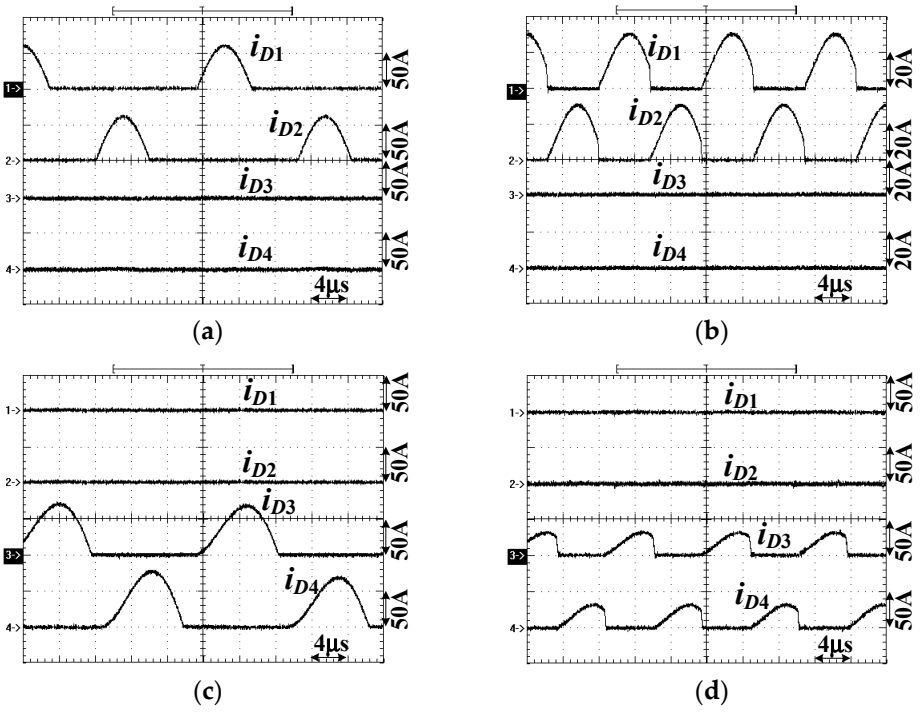

Figure 8. Measured results of the secondary side diode currents at rated power values of: (**a**) V_{in} = 100 V; (**b**) V_{in} = 190 V; (**c**) V_{in} = 210 V; (**d**) V_{in} = 400 V.

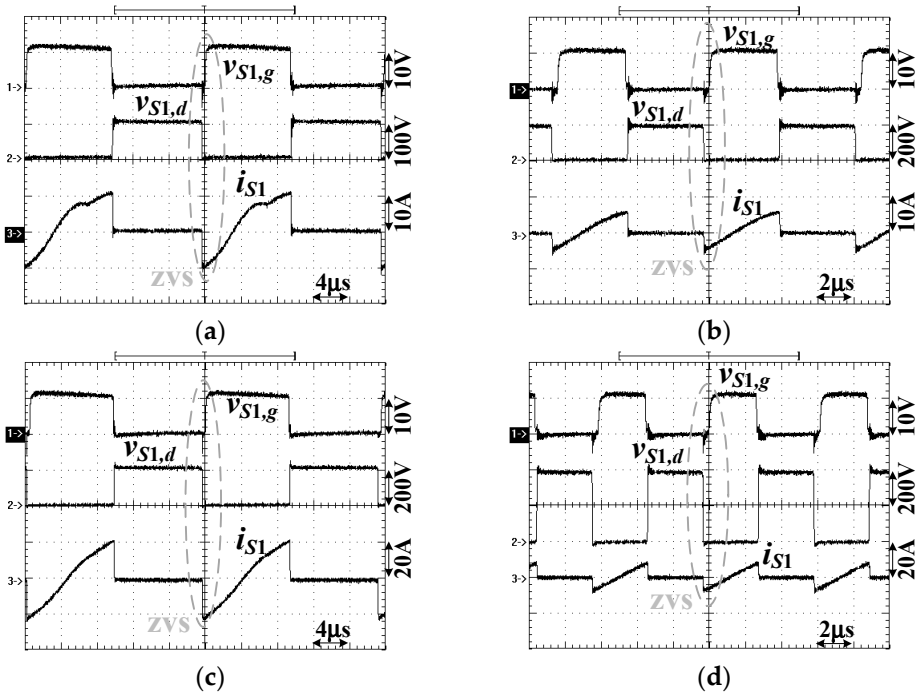

Figure 9. Measured results of $v_{S1,g}$, $v_{S1,d}$, and i_{S1} at 20% power; (**a**) V_{in} = 100 V; (**b**) V_{in} = 190 V; (**c**) V_{in} = 210 V; (**d**) V_{in} = 400 V.

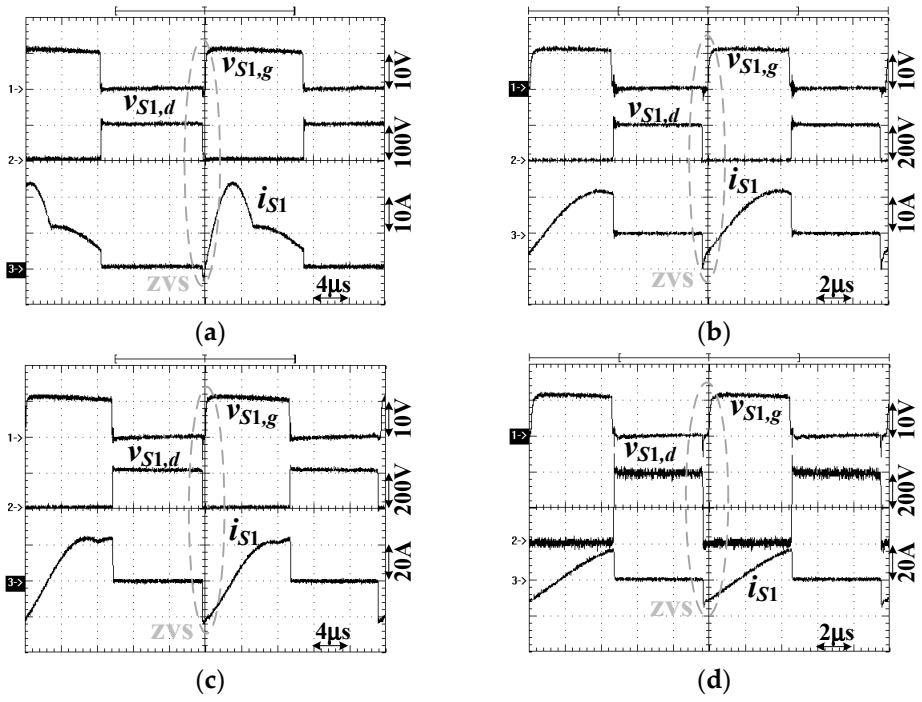

Figure 10. Measured results of $v_{S1,g}$, $v_{S1,d}$, and i_{S1} at the rated power values of: (**a**) V_{in} = 100 V; (**b**) V_{in} = 190 V; (**c**) V_{in} = 210 V; (**d**) V_{in} = 400 V.

The measured input voltage and the PWM signal of the AC switch S_{ac} are provided in Figure 11. The hysteresis voltage band and reference voltage of the voltage comparator are 10 V and 200 V, respectively. First, the input voltage is increased from 100 V to 400 V. When V_{in} is greater than 205 V, the PWM signal of S_{ac} is changed from the "on" state (high-voltage) to "off" state (low-voltage). Second, the input voltage is decreased from 400 V. When V_{in} is less than 195 V, S_{ac} is turned on

(high-voltage). Figure 12 gives the experimental switching frequency of the proposed resonant converter. For low-voltage ranges and the same load condition, the voltage gain of the resonant converter under V_{in} = 100 V is higher than V_{in} = 190 V. One can see that the measured switching frequency at 100 V input voltage is lower than 190 V input voltage. The experimental circuit efficiencies of the proposed converter at 100% load are 87.3% (100 V input), 91.2% (190 V input), 89.5% (210 V input), and 92.8% (400 V input). Since the turns ratio n_p/n_s is used under high-voltage ranges (V_{in} = 200–400 V) instead of $n_p/(2n_s)$ under low-voltage ranges (V_{in} = 100–200 V), the converter has a lower magnetizing current under high-voltage ranges compared to the low-voltage range operation. The converter has lower conduction loss on power switches at high-input voltage ranges. Therefore, the experimental circuit efficiency at 400 V input is better than the 190 V input, and the efficiency with the 210 V input is better than the 100 V input.

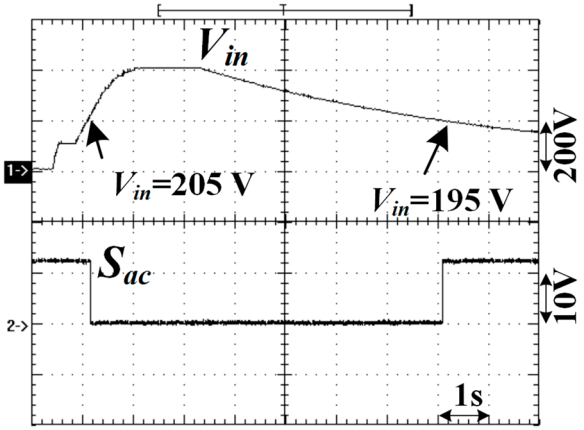

Figure 11. The experimental waveforms of the input voltage V_{in} and PWM signal of S_{ac}.

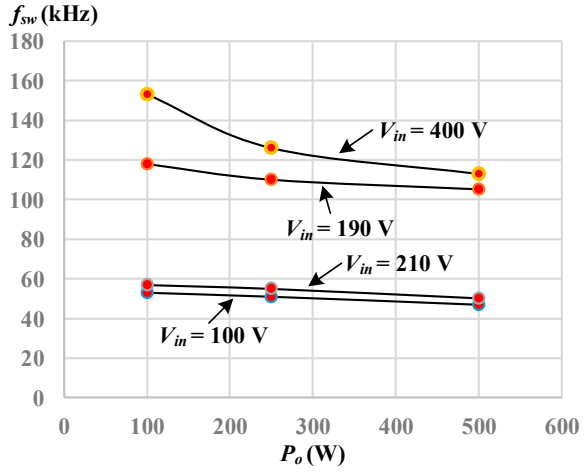

Figure 12. Measured switching frequency under various input voltages and load conditions.

5. Conclusions

The half-bridge LLC resonant converter with variable winding turns is studied and implemented in this paper to accomplish two objectives: (1) wide, soft switching ranges over the entire input voltage and output road; and (2) wide voltage operation. The general half-bridge resonant converter is adopted on the high-voltage side to a achieve series resonant circuit and realize the soft switching operation for powered semiconductors. Two sets of winding turns are adopted on the low-voltage side to accomplish wide voltage operation capability. Based on the circuit analysis and test results, the proposed LLC converter can achieve zero voltage switching with wide input voltage (100 V to 400 V) and wide load

(20% to 100% rated power) ranges. Compared to the conventional LLC resonant converters with wide voltage operation, the proposed converter has lower component counts, a simple control scheme, and less voltage stress on rectifier diodes. The studied LLC converter can be used for power units in computers and power servers with large hold-up times, PV power converters, fuel cell converters, and battery chargers and dischargers with wide voltage operation. Experimental waveforms from a 500 W prototype are given and presented to confirm the usefulness of the presented circuit topology. The future works will investigate the new wide voltage converters with low cost and high power density advantages for industry power applications and renewable energy power conversion.

Author Contributions: B.-R.L. proposed and designed this project and was responsible for writing the paper. C.-X.D. measured the circuit waveforms in the experiment. All authors have read and agreed to the published version of the manuscript.

Funding: This research is funded by the Ministry of Science and Technology, Taiwan, under grant number MOST 108-2221-E-224-022-MY2.

Acknowledgments: This work is supported by the Ministry of Science and Technology, Taiwan (MOST 108-2221-E-224-022-MY2). In addition, the authors are grateful to the all the editor and the reviewers for their valuable suggestions to improve this paper.

Conflicts of Interest: The author declares no conflict of interest.

References

1. Kim, J.Y.; Kim, H.S.; Baek, J.W.; Jeong, D.K. Analysis of effective three-level neutral point clamped converter system for the bipolar LVDC distribution. *Electronics* **2019**, *8*, 691. [CrossRef]
2. Blaabjerg, F.; Dragicevic, T.; Davari, P. Applications of Power Electronics. *Electronics* **2019**, *8*, 465. [CrossRef]
3. Almalaq, Y.; Matin, M. Three topologies of a non-isolated high gian switched-capacitor step-up cuk converter for renewable energy applications. *Electronics* **2018**, *7*, 94. [CrossRef]
4. Tahir, S.; Wang, J.; Balocj, M.H.; Kaloi, G.S. Digital control techniques based on voltage source inverters in renewable energy applications: A review. *Electronics* **2018**, *7*, 18. [CrossRef]
5. Lin, B.R. Phase-shift pwm converter with wide voltage operation capability. *Electronics* **2020**, *9*, 47. [CrossRef]
6. Lin, B.R. Analysis of a dc converter with low primary current loss and balance voltage and current. *Electronics* **2019**, *8*, 439. [CrossRef]
7. Kamal, T.; Karabackk, M.; Hassan, S.Z.; Fernández-Ramírez, L.M.; Riaz, M.H.; Riaz, M.T.; Khan, M.A.; Khan, L. Energy management and switching control of PHEV charging stations in a hybrid smart micro-grid system. *Electronics* **2018**, *7*, 156. [CrossRef]
8. Wang, P.; Zhou, L.; Zhang, Y.; Li, J.; Sumner, M. Input-parallel output-series DC-DC boost converter with a wide input voltage range, for fuel cell vehicles. *IEEE Trans. Vehicular Tech.* **2017**, *66*, 7771–7781. [CrossRef]
9. Lin, B.R.; Hsieh, F.Y. Soft-switching zeta-flyback converter with a buck-boost type of active clamp. *IEEE Trans. Ind. Electron.* **2007**, *54*, 2813–2822.
10. Jeong, Y.; Park, J.D.; Moon, G.W. An interleaved active-clamp forward converter modified for reduced primary conduction loss without additional components. *IEEE Trans. Power Electron.* **2020**, *35*, 121–130. [CrossRef]
11. Lin, B.R.; Chao, C.H. A new ZVS DC/DC converter with three APWM circuits. *IEEE Trans. Ind. Electron.* **2013**, *60*, 4351–4358. [CrossRef]
12. Pont, N.C.D.; Bandeira, D.; Lazzarin, T.B.; Barbi, I. A ZVS APWM half-bridge parallel resonant DC–DC converter with capacitive output. *IEEE Trans. Ind. Electron.* **2019**, *66*, 5231–5241. [CrossRef]
13. Mishima, T.; Akamatsu, K.; Nakaoka, M. A high frequency-link secondary-side phase-shifted full-bridge soft-switching PWM DC-DC converter with ZCS active rectifier for EV battery charger. *IEEE Trans. Power Electron.* **2013**, *28*, 5758–5773. [CrossRef]
14. Pahlevaninezhad, M.; Das, P.; Drobnik, J.; Pain, P.K.; Bakhshai, A. A novel ZVZCS full-bridge DC/DC converter used for electric vehicles. *IEEE Trans. Power Electron.* **2012**, *27*, 2752–2769. [CrossRef]
15. Steigerwald, R.L. A comparison of half-bridge resonant converter topologies. *IEEE Trans. Power Electron.* **1988**, *3*, 174–182. [CrossRef]

16. Lin, B.R.; Chu, C.W. Hybrid full-bridge and LLC converter with wide ZVS range and less output inductance. *IET Power Electron.* **2016**, *9*, 377–384. [CrossRef]
17. Yang, G.; Dubus, P.; Sadarnac, D. Double-phase high-efficiency, wide load range high-voltage/low-voltage LLC DC/DC converter for electric/hybrid vehicles. *IEEE Trans. Power Electron.* **2015**, *30*, 1876–1886. [CrossRef]
18. Lee, J.B.; Kim, J.K.; Baek, J.I.; Kim, J.H.; Moon, G.W. Resonant capacitor on/off control of half-bridge LLC converter for high efficiency server power supply. *IEEE Trans. Ind. Electron.* **2016**, *63*, 5410–5415. [CrossRef]
19. Lu, J.; Kumar, A.; Afridi, K.K. Step-down impedance control network resonant DC-DC converter utilizing an enhanced phase-shift control for wide-input-range operation. *IEEE Trans. Ind. Appl.* **2018**, *54*, 4523–4536. [CrossRef]
20. Hu, H.; Fang, X.; Chen, F.; Shen, Z.J.; Batarseh, I. A modified high-efficiency LLC converter with two transformers for wide input-voltage range applications. *IEEE Trans. Power Electron.* **2013**, *28*, 1946–1960. [CrossRef]
21. Sun, W.; Xing, Y.; Wu, H.; Ding, J. Modified high-efficiency LLC converters with two split resonant branches for wide input-voltage range applications. *IEEE Trans. Power Electron.* **2018**, *33*, 7867–7870. [CrossRef]
22. Jeong, Y.; Kim, J.K.; Lee, J.B.; Moon, G.W. An asymmetric half-bridge resonant converter having a reduced conduction loss for DC/DC power applications with a wide range of low-input voltage. *IEEE Trans. Power Electron.* **2017**, *32*, 7795–7804. [CrossRef]
23. Lin, B.R. Implementation of a Parallel-Series Resonant Converter with Wide Input Voltage Range. *Energies* **2019**, *12*, 4095. [CrossRef]
24. Lin, B.R. Resonant converter with soft switching and wide voltage operation. *Energies* **2019**, *12*, 3479. [CrossRef]
25. Lin, B.R. Resonant converter with wide input voltage range and input current ripple free. *IET Proc. Electron. Lett.* **2018**, *54*, 1086–1088. [CrossRef]
26. Lin, B.R. Series resonant converter with auxiliary winding turns: Analysis, design and implementation. *Int. J. Electron.* **2018**, *105*, 836–847. [CrossRef]